Numerical Simulation of High Reynolds Number Transonic Flows

George S. Deiwert*
NASA Ames Research Center, Moffett Field, Calif.

A code has been developed for simulating high Reynolds number transonic flowfields of arbitrary configuration. An explicit finite-difference method with time splitting is used to solve the time-dependent equations for compressible turbulent flow. A nonorthogonal computation mesh of arbitrary configuration facilitates the description of the flowfield. The code is applied to simulate the flow over an 18% thick circular-arc biconvex airfoil at zero angle of attack and $M_\infty = 0.775$. A simple mixing-length model is used to describe the turbulence and chord Reynolds numbers of 1, 2, 4, and 6.67 million are considered. The solution describes in detail both the shock-induced and trailing-edge separation regions, and provides the profile and friction drag.

Introduction

HIGH Reynolds number transonic flows exhibit serveral features that are important to aerodynamic design. Transonic flow past an airfoil in a subsonic freestream contains a supersonic flow region somewhere between the leading and trailing edge. This supersonic flow becomes subsonic by passing through a standing shock. If the shock strength is large enough, boundary-layer separation will occur. Depending on the airfoil configuration, there may be separation at the trailing edge that can coalesce with the shock-induced separation region. To complicate further the analysis of such flows, the boundary layer on the airfoil surface is generally turbulent and its response to strong adverse pressure gradients may be a function of Reynolds number.

In an attempt to study such flowfields and assess the influence of Reynolds number, the flow over a two-dimensional 18% thick circular-arc biconvex airfoil at zero angle of attack is simulated for chord Reynolds numbers of 1, 2, 4, and 6.67×10^6, and a freestream Mach number of 0.775. The explicit predictor-corrector finite-difference method with time splitting developed by MacCormack[1] has been generalized to flows of arbitrary geometry and is used to solve the two-dimensional time-dependent equations of motion governing the flow.

Analysis

Governing Equations

The flowfield is described by the two-dimensional time-dependent compressible equations of motion for turbulent flow. Written in integral form, they are

$$\frac{\partial}{\partial t}\int_{\text{vol}} U \, d\,\text{vol} + \int_S \boldsymbol{H}\cdot\boldsymbol{n}\,ds = 0 \tag{1}$$

where

$$U \equiv \begin{bmatrix} \rho \\ \rho u \\ \rho v \\ e \end{bmatrix} \qquad \boldsymbol{H} \equiv \begin{bmatrix} \rho \boldsymbol{q} \\ \rho u \boldsymbol{q} + \boldsymbol{\tau}\cdot\boldsymbol{e}_x \\ \rho v \boldsymbol{q} + \boldsymbol{\tau}\cdot\boldsymbol{e}_y \\ e\boldsymbol{q} + \boldsymbol{\tau}\cdot\boldsymbol{q} - k\Delta T \end{bmatrix}$$

$$\boldsymbol{q} \equiv u\boldsymbol{e}_x + v\boldsymbol{e}_y$$

$$\boldsymbol{\tau} \equiv \sigma_x \boldsymbol{e}_x\boldsymbol{e}_x + \tau_{xy}\boldsymbol{e}_x\boldsymbol{e}_y + \tau_{yx}\boldsymbol{e}_y\boldsymbol{e}_x + \sigma_y\boldsymbol{e}_y\boldsymbol{e}_y$$

and $\boldsymbol{e}_x$, $\boldsymbol{e}_y$ are unit vectors, and $\boldsymbol{n}$ is a unit normal vector. These equations can be solved in the orthogonal x,y coordinate system for an arbitrary quadrilateral volume element (Fig. 1) by application of the split Ly and Lx operators in the manner described by MacCormack.[2]

Ly operator:

$$\text{predictor}\quad \overline{U_{i,j}^{n+1/2}} = U_{i,j}^n - (\Delta t/\text{vol}_{i,j}) \times (\boldsymbol{H}_{i,j}^n \cdot \boldsymbol{S}_3 + \boldsymbol{H}_{i,j-1}^n \cdot \boldsymbol{S}_1)$$

$$\text{corrector}\quad U_{i,j}^{n+1/2} = \tfrac{1}{2}[U_{i,j}^n + \overline{U_{i,j}^{n+1/2}} - (\Delta t/\text{vol}_{i,j}) \times (\overline{\boldsymbol{H}_{i,j+1}^{n+1/2}} \cdot \boldsymbol{S}_3 + \overline{\boldsymbol{H}_{i,j}^{n+1/2}} \cdot \boldsymbol{S}_1)]$$

Lx operator:

$$\text{predictor}\quad \overline{U_{i,j}^{n+1}} = U_{i,j}^{n+1/2} - (\Delta t/\text{vol}_{i,j}) \times (\boldsymbol{H}_{i,j}^{n+1/2} \cdot \boldsymbol{S}_4 + \boldsymbol{H}_{i-1,j}^{n+1/2} \cdot \boldsymbol{S}_2)$$

$$\text{corrector}\quad U_{i,j}^{n+1} = \tfrac{1}{2}[U_{i,j}^{n+1/2} + \overline{U_{i,j}^{n+1}} - (\Delta t/\text{vol}_{i,j}) \times (\overline{\boldsymbol{H}_{i+1,j}^{n+1}} \cdot \boldsymbol{S}_4 + \overline{\boldsymbol{H}_{i,j}^{n+1}} \cdot \boldsymbol{S}_2)]$$

where the superscript n denotes the time step index, and the subscripts i and j are the spatial index in the x and y direction, respectively. The Ly and Lx operators are applied so that Eq. (1) is satisfied at each time step for each cell of the nonorthogonal computational mesh. To evaluate the viscous derivatives for the nonorthogonal mesh, the following transformation is appropriate:

$$\frac{\partial\phi}{\partial x} = \frac{\partial\phi}{\partial\xi}\frac{\partial\xi}{\partial x} + \frac{\partial\phi}{\partial\eta}\frac{\partial\eta}{\partial x}$$

$$\frac{\partial\phi}{\partial y} = \frac{\partial\phi}{\partial\xi}\frac{\partial\xi}{\partial y} + \frac{\partial\phi}{\partial\eta}\frac{\partial\eta}{\partial y}$$

where ϕ is a dummy-dependent variable, and (ξ,η) are the local coordinates of the nonorthogonal mesh. In terms of the notation in Fig. 2,

$$\frac{\partial\phi}{\partial x} = \frac{\Delta\phi_\xi \Delta y_\eta - \Delta\phi_\eta \Delta y_\xi}{\Delta x_\xi \Delta y_\eta - \Delta x_\eta \Delta y_\xi} \times \frac{\partial\phi}{\partial y} = \frac{\Delta\phi_\xi \Delta x_\eta - \Delta\phi_\eta \Delta x_\xi}{\Delta y_\xi \Delta x_\eta - \Delta y_\eta \Delta x_\xi}$$

Presented as Paper 74-603 at the AIAA 7th Fluid and Plasma Dynamics Conference, Palo Alto, California, June 17-19, 1974; submitted October 25, 1974; revision received March 10, 1975.

Index categories: Subsonic and Transonic Flow; Boundary Layers and Convective Heat Transfer—Turbulent; Computer Technology and Computer Simulation Techniques.

*Research Scientist.

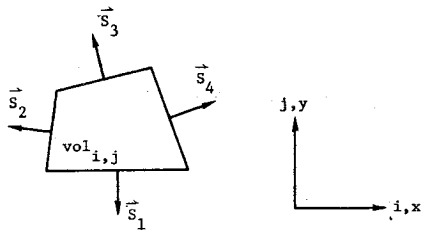

Fig. 1 Quadrilateral volume element.

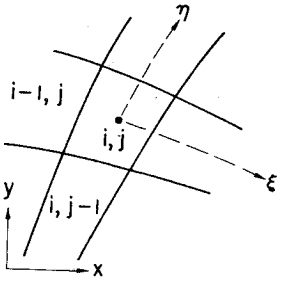

Fig. 2 Nonorthogonal mesh notation.

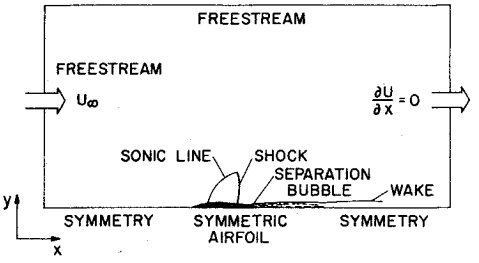

Fig. 3 Computational control volume.

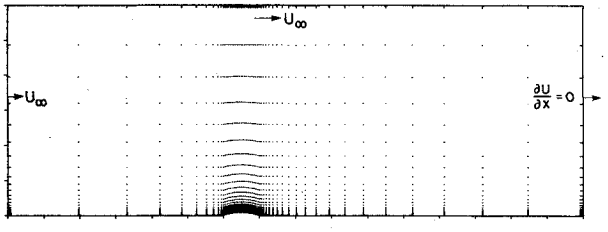

Fig. 4 Mesh configuration for 18% circular-arc.

For evaluation on surfaces S_3 and S_4, the differences are defined as

$$\Delta\phi_\xi = \phi_{i+1,jj} - \phi_{im,jj} \qquad \Delta\phi_\eta = \phi_{ii,j+1} - \phi_{ii,jm}$$

$$\Delta x_\xi = x_{i+1,jj} - x_{im,jj} \qquad \Delta x_\eta = x_{ii,j+1} - x_{ii,jm}$$

$$\Delta y_\xi = y_{i+1,jj} - y_{im,jj} \qquad \Delta y_\eta = y_{ii,j+1} - y_{ii,jm}$$

and

$$im = \begin{cases} i & \text{for } Lx \\ i-1 & \text{for } Ly \end{cases} \qquad ii = \begin{cases} i \\ i+1 & \text{for } Lx \text{ corrector} \end{cases}$$

$$jm = \begin{cases} j-1 & \text{for } Lx \\ j & \text{for } Ly \end{cases} \qquad jj = \begin{cases} j \\ j+1 & \text{for } Ly \text{ corrector} \end{cases}$$

This treatment of the viscous derivatives always results in centered differences, maintains second-order accuracy, and provides consistent treatment of discontinuous boundary conditions (such as at the leading and trailing edges of the airfoil).

Control Volume, Mesh, and Boundary Condtions

An 18% thick circular-arc biconvex airfoil, initially at rest, is impulsively started at time zero at the desired freestream Mach number and pressure. Figure 3 shows a typical control volume for which the flowfield development is followed in time. At a sufficient distance upstream of the leading edge (in this case 6 chord lengths), the flow is assumed uniform at the freestream conditions ($u=U_\infty$, $v=0$) as it is along the far transverse boundary (again, 6 chord lengths away). The downstream boundary is positioned far enough downstream of the trailing edge (9 chord lengths) so that all gradients in the flow direction may be assumed negligible ($\partial\phi/\partial x=0$). The surface of the airfoil is impermeable and "no slip" boundary conditions are assumed ($u=v=0$). The airfoil is assumed adiabatic ($\nabla T\cdot n=0$) and the normal surface pressure gradient is zero ($\partial p/\partial n=0$). The zero normal surface pressure gradient assumption is a boundary-layer approximation and is not rigorous for the full compressible Navier-Stokes equations used in the present study. It is used here, however, because of its simplicity and, because studies by the present author and by MacCormack and Baldwin[8] indicate that for the type mesh used here it is totally adequate. Ahead of and behind the airfoil, the flow is symmetric. Because the airfoil is thick and the flowfield is transonic, boundary-layer separation is likely. To simulate this phenomenon reliably for turbulent flow it is necessary to resolve the boundary layer to the sublayer scale. This sublayer scale is nearly proportional to $1/(Re_c)^{1/2}$ so that, for the high Reynolds number flows of interest, the mesh resolution near the surface must be extremely fine. As a rule of thumb, a first mesh spacing of $\Delta y_{\min} = 2/3\ [c/(\mathrm{Re}_c)^{1/2}]$ is adequate.

A 50×38 mesh is shown in Fig. 4. In the x-direction, the mesh is uniformly distributed over the surface of the airfoil (20 points) and is exponentially stretched ahead of (10 points) and behind (20 points) the airfoil. In the y-direction, a coarse mesh of 26 points is exponentially stretched away from the airfoil. The innermost region is further subdivided into a medium mesh of 10 exponentially stretched points and a fine mesh of 4 uniformly spaced points. The rather coarse mesh used in the flow direction is not capable of supporting high resolution in regions of relatively large streamwise gradients such as through a shock or at the onset of separation. Special techniques such as shock fitting may be used to define more precisely the location of standing shock waves, but nothing short of many more mesh points will suffice to resolve all the flowfield details completely at the onset of separation and reattachment. The coupling between the inviscid and viscous flow regions, however, is maintained, as is the range of pressure variation in the interaction region. The lack of rigorous turbulent transport models does not warrant the added cost of high resolution in the streamwise direction at this time.

Turbulence Model

For expediency a simple mixing-length model[3] is used to describe the turbulent transport, which for boundary-layer flow is given by

$$\epsilon = \rho\ell^2\,|(\partial u/\partial y) + (\partial v/\partial x)|$$

where

$$\ell = 0.4\,y\left[1-\exp\left(-y/26\left[\left|\frac{\rho}{\mu}\frac{\partial u}{\partial y}\right|_w\right]^{1/2}\right)\right]$$

for the inner region, and y is measured from the point of zero tangential velocity; $\ell = 0.07\,\delta$ for the outer flow, and δ is determined from an arbitrary cutoff in the vorticity field. For the wake region, the turbulent viscosity is given by

$$\epsilon = 0.001176\rho\delta\,|u_\delta - u_\ell|$$

where u_δ and u_ℓ are the velocities at the edge of the wake and its centerline, respectively. Using this model, the shear stress terms may be determined by

$$\tau = \tau_{xy} = \tau_{yx} = (\mu + \epsilon)\,[\,(\partial u/\partial y) + (\partial v/\partial x)\,]$$

This turbulence model is believed to be adequate for the attached boundary layer ahead of the shock and for the wake flow downstream of the reattachment point. Its validity in the separated flow region is highly suspect, however, and requires verification by experiment. While it may be necessary to resort to more rigorous turbulent models for the separated region, the simple model used here should permit some insight into the influence of Reynolds number on such flowfields.

Computational Time Step

Six different computational time steps are used in the calculation; one for the Lx operator and one for the Ly operator in each of the three mesh regions in the y-direction. Each time step is determined by the CFL and viscous stability requirements from the following relation:

$$\Delta t = h/[\,|V| + a + (\alpha/h)\;(\mu+\epsilon)/\rho]$$

where h is the appropriate mesh spacing, V is the appropriate velocity component, a is the local speed of sound, and α is a function of the mesh aspect ratio. In the fine mesh in the wake behind the airfoil, the eddy viscosity ϵ is quite large, and the viscous stability criterion may govern the time step for the Ly operator. To avoid this undesirable restriction and unneeded resolution of the wake, the entire fine mesh region downstream of the airfoil is averaged and treated as part of the medium mesh.

Computer Requirements

The present code was originally written in FORTRAN and debugged on an IBM 360/67 using the interactive features of the time sharing system. Subsequently, it was run on the CDC 7600, requiring 2-10 hrs per converged solution, depending on chord Reynolds number. Convergence for the present solutions was assumed after the mean flow traveled 7.5 chords. Because of the long run times the code was completely restructured and written in the vector-oriented Ames-developed CFD language.[13] This code was translated to assembly language for the ILLIAC IV and to FORTRAN for the CDC 7600. The resulting FORTRAN code was further optimized, using COMPASS coded subroutines for *all* vector arithmetic operations. Resultant run times are now 0.8-4.2 hr per converged solution on the CDC 7600, and 0.6-3.0 hr on the ILLIAC IV. There is substantial room for speed increase on the ILLIAC IV in that 1) the quoted run times were for the ILLIAC operating at 11.5 MHz instead of the design speed of 15-16 MHz, 2) the ILLIAC was operated in nonoverlap mode, and 3) each iteration was performed twice and the solutions compared before continuing with the computation. Each of these areas represents potential speed reductions of 0.72, 0.40, and 0.48 respectively, leading to an overall potential speed reduction of 0.14. In this case the present code would require 0.08-0.42 hr per converged solution—an order of magnitude faster than the vector coded CDC 7600.

Validation

Because computations of this complexity have not previously been performed, the validity of the present code has been determined by comparison with established computations for certain specific regions of the flowfield and with experimental results obtained in the Ames High Reynolds Number Channel. First, the viscous terms were neglected and the inviscid flow over a 6% circular-arc airfoil at a freestream Mach number of 0.90 was computed. The surface pressure distribution is compared in Fig. 5 with a computation using the program of E. M. Murman[4-7] and a computation by R. W. MacCormack.[8] Both these reference computations employed "shock fitting," which has not yet been incorporated in the present code. The agreement between the three computations (all of which solve the conservative form of the equations) is excellent.

Second, the flow over an 18% thick circular-arc airfoil at a freestream Mach number of 0.775 and a chord Reynolds number of 2×10^6 was computed. Figure 6 shows a comparison with experiment[9] for surface pressure distribution. Two computed distributions are included as determined by the present code. One of these is an inviscid calculation and the other is determined using the eddy-viscosity model described previously. All comparisons are in excellent agreement ahead of the interaction region. The viscous computation shows a marked improvement over the inviscid results in the interaction region but still is not in good agreement with experiment. The viscous solution indicates a shock-induced separation with the separation bubble extending into the wake. This is denoted in Fig. 6 by the pressure plateau downstream of the 80% chord point. The experimental pressure distribution does not indicate this extensive separation region and herein constitutes the greatest disagreement between computation and experiment. The preliminary experimental results to date indicate that, at this particular choice of freestream Mach number, the experimental flowfield can be highly unsteady, alternating between shock-induced and trailing-edge-only separation. This buffeting phenomenon invalidates direct comparisons in the separated flow region. At lower Mach numbers, the experimental flowfield is steady with only trailing-edge separation, and at higher Mach numbers the experimental flowfield is steady with shock-induced separation, as indicated by the viscous computations. While the present mixing length model may be adequate to describe the attached boundary-layer and wake-flow regions, more sophisticated turbulence models may be required to permit

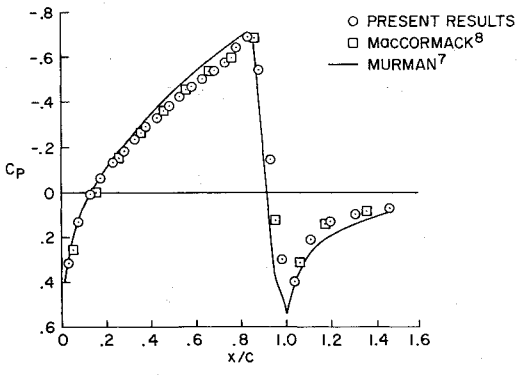

Fig. 5 Inviscid pressure distribution over 6% circular-arc; $M_\infty = 0.90$.

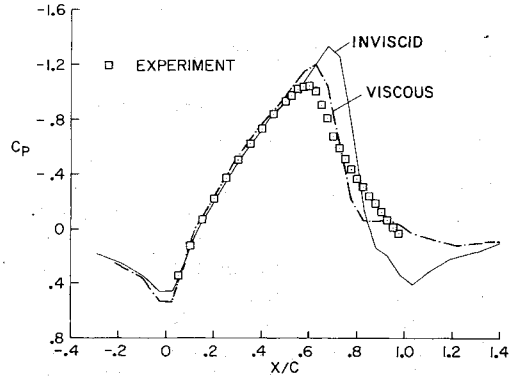

Fig. 6 Pressure distribution over 18% circular-arc; $M_\infty = 0.775$, $Re_c = 2\times10^6$.

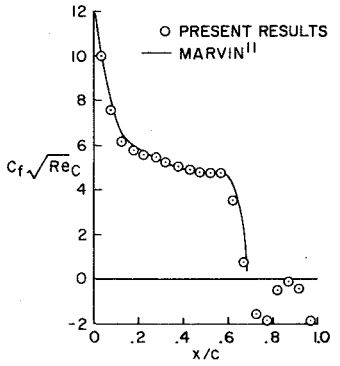

Fig. 7 Skin-friction distribution over 18% circular-arc; $M_\infty = 0.775$, $Re_c = 2 \times 10^6$.

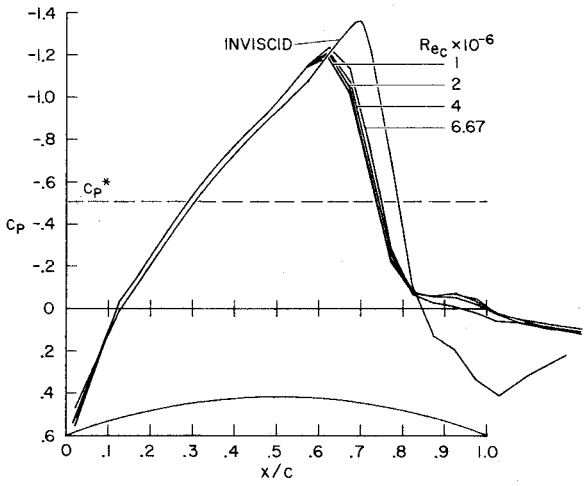

Fig. 8 Pressure distribution over 18% circular-arc; $M_\infty = 0.775$.

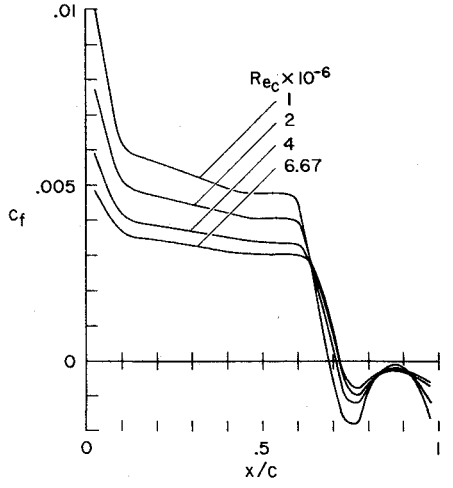

Fig. 9 Skin-friction distribution over 18% circular-arc; $M_\infty = 0.775$.

adequate description of this Mach number dependence on the viscous-inviscid interaction region.

Third, the previous computed pressure distribution was used as input in the turbulent boundary-layer code of Marvin and Sheaffer,[10,11] which uses an implicit Crank-Nicholson method and a Cebeci-Smith eddy viscosity model.[12] Computed values of local skin friction from this code are compared with the present calculations in Fig. 7. Ahead of the separated flow region the agreement is excellent except for a small region near the leading edge, where the Marvin-Sheaffer code assumes a laminar to turbulent transition region.

The excellent agreement indicated in the previous three cases is sufficient to warrant using the computer code to study

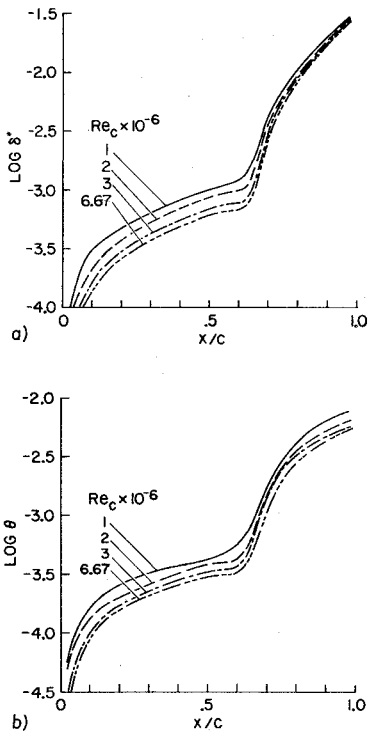

Fig. 10 Thickness parameters on 18% circular-arc; $M_\infty = 0.775$: a) Displacement thickness; b) Momentum thickness.

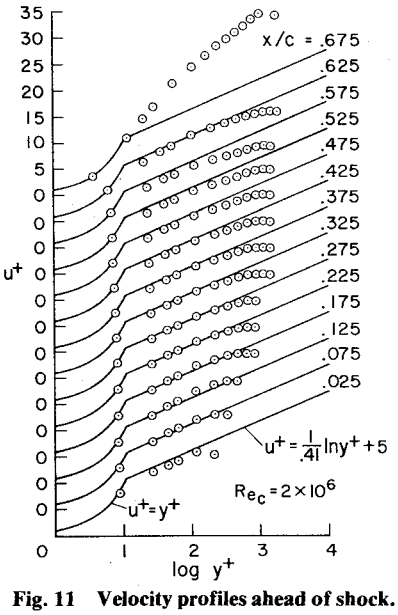

Fig. 11 Velocity profiles ahead of shock.

separated viscous flows. The results for four such flowfields are described in the following section.

Results

Flowfield solutions for the 18% thick circular-arc airfoil were computed for Reynolds numbers of $Re_c = 1$, 2, 4, and 6.67×10^6 for a freestream Mach number of 0.775. All solutions were carried out for a time corresponding to the mean flow traveling 7.5 chord lengths, and convergence to steady state was determined by monitoring the stress tensor on the body surface, and in the near wake.

Figure 8 shows the pressure coefficient variation over the airfoil surface. The inviscid pressure distribution is included for comparison. All the viscous solutions lie to the left of the inviscid solution because of boundary-layer displacement effects. The effect is most pronounced for the shock location

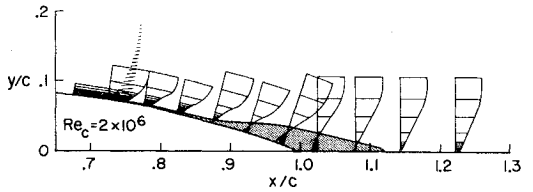

Fig. 12 Separation velocity profiles on 18% circular-arc; $M_\infty = 0.775$.

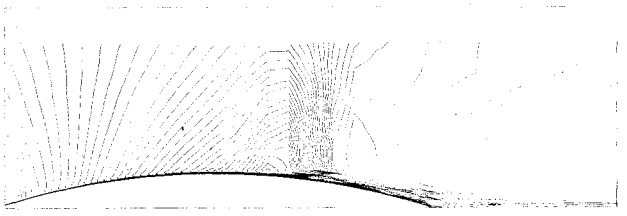

Fig. 13 Mach number contours; $M_\infty = 0.775$; $Re_c = 4\times10^6$.

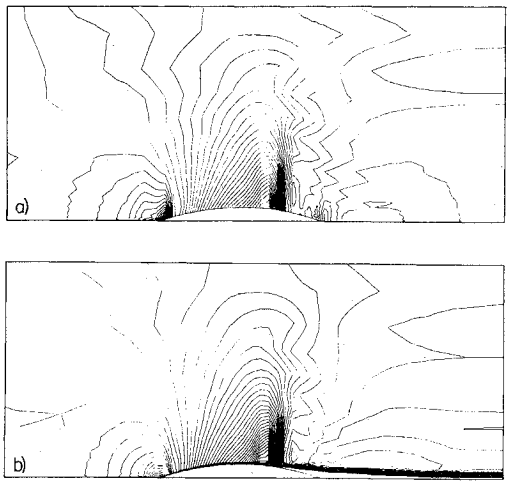

Fig. 14 Flowfield contours; $M_\infty = 0.775$; $Re_c = 6.67\times10^6$, 18% circular-arc: a) Isobars; b) Mach number.

because of flow separation predicted at the shock in the viscous solutions. At the trailing edge, the viscous pressure distributions form a plateau in the long separation bubble region. As the Reynolds number is decreased, the shock strength decreases and the shock moves farther upstream on the airfoil. This is a result of the lower Reynolds number boundary layers being thicker, having less momentum, and thus being more susceptible to separation. Decreasing Reynolds number also is accompanied by a decrease in pressure recovery behind the shock, indicating greater displacement effects in the separated region. For the particular geometry under consideration, the influence of Reynolds number on surface pressure distribution is not great but is in the direction intuitively predicted. For the range of Reynolds numbers considered here, the shock is centered (where $c_p = c_p{}^*$) between the 73 and 75% chord.

Figure 9 shows the skin-friction variation over the airfoil surface. Ahead of the shock, as the Reynolds number is decreased the skin-friction coefficient is increased. Separation occurs farther upstream for the lower Reynolds number flows and, for the four Reynolds numbers considered, begins between the 69 and 72% chord, some 3% chord ahead of the centered shock location indicated in Fig. 8. After the shock-induced separation region; the flow tends to reattach but merges with the trailing-edge separation region. Note that the skin-friction coefficient distribution for the lowest Reynolds number exhibits the widest variation in the separation region and, in fact, almost reattaches before the trailing-edge separation region. This variation in skin-friction coefficient distribution becomes less pronounced as the Reynolds number is increased.

Figures 10a and 10b show variations of displacement and momentum thicknesses, respectively. Both thickness parameters increase with decreasing Reynolds number and vary by more than two orders of magnitude over the length of the airfoil. Just ahead of the shock-induced separation region, both thickness parameters begin increasing dramatically over the separation bubble. This thickening is due to the reverse flow near the airfoil surface.

Typical boundary-layer profiles ahead of the shock are compared in Fig. 11 with the compressible form of the universal "law of the wall" for the $Re_c = 2\times10^6$ solution. Here the symbols represent the numerical solution and are plotted at y^+ values corresponding to the mesh centers. All profiles are seen to have one point in the sublayer and adequately describe the log-law and wake flow regions of the boundary layer. By having at least one point in the sublayer, both the skin-friction distribution and separation phenomena can be described.

Velocity profiles in the separation region are shown in Fig. 12 for the $Re_c = 2\times10^6$ solution. These profiles are plotted in the physical coordinate system over the aft portion of the airfoil and are extended on into the wake where the separation bubble is seen to close. The first separated profile, which is plotted on a scale much larger than the initial separation thickness, is at 0.725 chord, indicating separation somewhat ahead of this point. The shock location is just downstream of this profile, centered about the 0.740-chord point. The reattachment point is nearly 0.1 chord downstream of the trailing edge. Figure 12 shows the dividing streamline within which the net mass flow is zero. Solution details for the separated region are similar for the other three cases.

Figure 13 is a Mach line contour plot near the surface of the airfoil. Contours are shown for $0 \le M \le 1.4$ in increments of 0.02 for $Re_c = 4\times10^6$. Thickening of the boundary layer as it progresses down the airfoil is clearly indicated. Near 70% chord, the shock impinges on the boundary layer and the flow separates, resulting in large displacement effects. Large transverse gradients in the boundary layer are seen to decrease as the flow progresses into the wake and longitudinal gradients become negligible. Inside the separation bubble, the gradients are much smaller than in the boundary layer or the near wake, indicating a lower speed and nearly incompressible flow.

Figure 14a shows the isobars and Fig. 14b the Mach lines of the inviscid flowfield for $Re_c = 6.67\times10^6$. These figures clearly indicate the position of the standing shock; in Fig. 14 b the boundary layer, wake, and separation bubble at the trailing edge are apparent. The isobars are shown for $0.46 \le p/p_\infty \le 1.32$ in increments of 0.02 and the Mach lines for $0.40 \le M \le 1.40$ in increments of 0.02. Both the forward and two rearward stagnation regions are indicated on the isobar plot on the symmetric boundary near the center of the innermost isobar arches. The smeared shock discontinuity is attributed to viscosity in conjunction with a coarse mesh spacing in the flow direction as well as an artificial fourth-order smoothinng term in the numerical algorithm.

Conclusions

The influence of Reynolds number on the transonic flowfield over an 18% thick circular-arc airfoil has been simulated. For increasing Reynolds number, the following trends have been established: 1) shock strength increases, 2) shock location moves rearward, 3) separation moves rearward, and 4) displacement effects decrease. While this Reynolds number effect is not great for the flowfield considered here, other airfoil configurations (such as supercritical airfoils) may be more sensitive.

No attempt was made in the present study to use a rigorous turbulence model. Since the flow is transonic, incompressible models should be accurate ahead of the separation region. In

the vicinity of the shock and in the separated flow region, however, the simple mixing-length model is highly suspect and flowfield details in these regions should be considered qualitative at this time.

References

[1]MacCormack, R. W., "Numerical Solution of the Interaction of a Shock Wave with a Laminar Boundary Layer," *Lecture Notes in Physics*, Vol. 8, Springer-Verlag, 1971, pp. 151-163.

[2]MacCormack, R. W. and Paullay, A. J., "Computational Efficiency Achieved by Time Splitting of Finite Difference Operators," AIAA Paper 72-154, San Diego, Calif., 1972.

[3]Launder, B. E., and Spalding, D. B., *Mathematical Models of Turbulence*, Academic Press, N.Y., 1972.

[4]Murman, E. M. and Cole, J. D., "Calculation of Plane Steady Transonic Flows," *AIAA Journal*, Vol. 9, Jan. 1971, pp. 114-121.

[5]Murman, E. M., "Analysis of Embedded Shock Waves Calculated by Relaxation Methods," *Proceedings of the AIAA Computational Fluid Dynamics Conference*, 1973, pp. 27-40.

[6]Murman, E. M., "Computation of Wall Effects in Ventilated Transonic Wind Tunnels," AIAA Paper 72-1007, Palo Alto, Calif., 1972, pp. 216-217.

[7]Murman, E. M., private communication, 1974, NASA Ames Research Center.

[8]MacCormack, R. W. and Baldwin, B. S., private communication, 1974, NASA Ames Research Center.

[9]McDevitt, J. B. and Levy, L. L., Jr., and Deiwert, G. S., "Transonic Flow about a Thick Circular-arc Airfoil," AIAA Paper 75-878, Hartford, Conn., 1975.

[10]Marvin, J. G. and Sheaffer, Y. S., "A Method for Solving the Nonsimilar Laminar Boundary-Layer Equations including Foreign Gas Injection," NASA TN D-5516, Nov. 1969.

[11]Marvin, J. G., private communication, 1974, NASA Ames Research Center.

[12]Inouye, M., Marvin, J. G., and Sheaffer, Y. S., "Turbulent-Wake Calculations with an Eddy-Viscosity Model," *AIAA Journal*, Vol. 10, Feb. 1972.

[13]Computational Fluid Dynamics Branch, "CFD-A FORTRAN-Based Language for the ILLIAC IV," internal paper, NASA Ames Research Center, 1973.